IEEE Access
Multidisciplinary ⋮ Rapid Review ⋮ Open Access Journal

Received October 14, 2020, accepted November 1, 2020, date of publication November 6, 2020, date of current version November 18, 2020.

Digital Object Identifier 10.1109/ACCESS.2020.3036592

Decentralized Control of Voltage- and Current-Controlled Converters Based on AC Bus Signaling for Autonomous Microgrids

LUCAS SAVOI DE ARAUJO[1], (Graduate Student Member, IEEE), AUGUSTO M. DOS SANTOS ALONSO[2,3], (Graduate Student Member, IEEE), AND DANILO IGLESIAS BRANDAO[1], (Member, IEEE)

[1]Graduate Program in Electrical Engineering, Federal University of Minas Gerais (UFMG), Belo Horizonte 31270-901, Brazil
[2]Department of Electric Power Engineering, Norwegian University of Science and Technology (NTNU), 7491 Trondheim, Norway
[3]Group of Automation and Integrated Systems, Sao Paulo State University (UNESP), Sorocaba 18087-180, Brazil

Corresponding author: Augusto M. dos Santos Alonso (augusto.alonso@ntnu.no)

This work was supported by the Department of Electric Power Engineering, Norwegian University of Science and Technology (NTNU), with Article Processing Charges (APC) funded by the NTNU Publishing Fund.

ABSTRACT This article proposes a fully decentralized control approach, based on AC bus signaling, to integrate the operation of voltage- and current-controlled converters that exist in an isolated low-voltage microgrid, so they may be fully steered under grid-feeding, grid-supporting, and grid-forming control principles. The proposed strategy, devised by classic and modified droop-based controllers, allows control of the microgrid active power relating to the system frequency, while regulating the reactive power related to the voltage, dispensing any need for communication infrastructures. Beyond ensuring proper microgrid power balance at all times, the control strategy prioritizes energy extraction from non-dispatchable sources (i.e., photovoltaic-based systems), whereas it uses dispatchable sources (i.e., battery-based systems) to share active and reactive power proportionally to their capabilities. As a consequence of the proper and novel management of battery-based converters, battery overvoltage and overcurrent are avoided, supporting a prolonged lifespan. Simulation results considering an autonomous microgrid operating under several scenarios are presented, to demonstrate the capabilities of the proposed control scheme on steering the different topologies of converters.

INDEX TERMS Battery energy storage systems, decentralized control, distributed generation, microgrids, power control.

I. INTRODUCTION

Power electronic converters are becoming key players on supporting the decentralization of electrical systems [1]. For example, they play an important role on ensuring compliant interface of renewable energy sources (RESs) of non-dispatchable nature (e.g., PV- and wind-based generation). Moreover, integration of dispatchable sources such as battery energy storage systems (BESSs) relies more and more on their use [2]. However, to adequately integrate multiple distributed sources that provide particular operational features, converters need to incorporate different control strategies according to their desired interactivity with the grid.

This is particular true for islanded AC microgrids (MGs), since they operate disconnected from the main grid and rely on autonomous control approaches to overcome many operational challenges. For instance, some challenges are the MG power balance and the adequate coordination of multiple converters that operate forming the grid, feeding loads, or simply dispatching active power [3]–[6]. Consequently, power converters are commonly designed to operate under current- or voltage-controlled modes [7], behaving as grid-forming (GFC), grid-supporting (GSC), or grid-feeding (GFdC) units [8], depending on their purpose. So, the

The associate editor coordinating the review of this manuscript and approving it for publication was Ziang Zhang.

following studies are highlighted to give grounds to this article, as well as to emphasize its novelties and contributions.

A. LITERATURE REVIEW

The decentralized coordination of current- and voltage-controlled converters in MGs (i.e., relying on communication-free approaches) has been widely explored in literature, mostly taking advantage of the conventional droop control [4]–[6], [9], [10]. However, many limitations are inherent to droop control, such as the difficulty to maintain power sharing accuracy along with proper regulation of voltage magnitude and frequency, as well as issues related to slow dynamics [5]. Additionally, when GFCs and GSCs interface BESSs in MGs, droop control is not commonly implemented with the capability of avoiding batteries overcurrent and overvoltage, as poor transient and steady-state controllability is inherent to the method [11]. Thus, to overcome the main operational limitations of conventional droop-based approaches, strategies like the adoption of virtual impedance loops [12]–[15], decentralized hierarchical control layers [5], [16], [17], and other novel strategies [18]–[21] have been studied.

The majority of works in literature, nevertheless, consider: *i*) only the existence of either current- or voltage-controlled converters in a MG; or *ii*) even if these two types of control topologies are modeled [7], the concern to provide concomitant support to the integration of GFCs, GSCs, and GFdCs is not commonly found. Additionally, the management of active and reactive power incorporating dispatchable and non-dispatchable sources in one strategy is scarce, considering that priorization of power generation from RESs is usually desired, and issues like overvoltages and overcurrents in BESSs need to be properly considered.

The concept of AC bus signaling [22], [23] is an approach that provides support to insert all these above-mentioned concerns within the management of droop-regulated autonomous MGs. By dynamically analyzing changes in AC bus voltage and frequency signals, droop-controlled converters being ruled under diversified control principles can automatically adjust their behaviors to achieve proper MG operation. Frequency bus signaling (FBS), for instance, is proposed in [24] and [25], being integrated to primary and secondary control layers to achieve frequency regulation, while preventing overcharging in BESSs operating under voltage-controlled mode. Nonetheless, the control topologies within [24] and [25] are not fully decentralized, the existence of GSCs is not considered, and the matter of reactive power sharing is not addressed.

FBS is also used in [23], along with smooth switching droop control, to achieve frequency regulation and to allow converters to seamlessly transit between power- and voltage-controlled modes. However, the operation of GFCs and GFdCs is not discussed considering the existence of GSCs. Shifting-frequency droop control has also been proposed for FBS control in [26], without supporting reactive power sharing capability. Similarly, frequency restoration is achieved in [27] by means of a small-AC-signal injection approach that maintains equalized real power sharing, without considering neither the existence of current-controlled converters, nor the presence of BESSs. Hierarchical control based on primary and secondary layers is proposed under a distributed approach in [28] to regulate voltage and frequency, although current-controlled converters are not modeled.

Conventional droop control accounting for regulation of BESS' voltage is presented in [29]. It is demonstrated that support to frequency and voltage amplitude regulation is achievable, while offering proper charging of BESSs. However, converters operating as GSCs are disregarded, and the method is subjected to non-accurate reactive power sharing due to mismatches in line impedances. Limitation in batteries overcurrent is neither addressed in [29], which may imply in battery damage.

With regards to the matter of power balance among RESs, BESSs and loads, FBS and frequency-voltage bus signaling can also be employed in autonomous MGs, as done respectively in [30] and [22]. Equalization of state-of-charge (SoC) is considered in such studies, along with the use of conventional droop control, allowing to achieve proper charging of BESSs. However, again, GSCs are not present in the MG control schemes. Power balance is discussed in [31] as well, being based on FBS and constant-voltage constant-frequency control, although only GFCs and GFdCs are considered, and focus is given to abnormal operation conditions of the MG, such as during short-term power shortage.

Finally, a summarized literature review is presented in Table 1, aiming at highlighting the different control topologies and converter operating modes found in major studies. Consequently, the contributions of this article can be more clearly presented as follows.

B. PAPER CONTRIBUTIONS AND ORGANIZATION

This article focuses on developing a fully decentralized control for the three types of converters (i.e., GFC, GFdC and GSC), taking into account the overvoltage and overcurrent limitations of battery banks. Thus, the main innovation is the battery overcurrent control for the GFC, and the control approach proposed for the GSC, which includes both battery overvoltage and overcurrent control functionalities. Taking into account the before-mentioned literature review, to the best of author's knowledge, such contributions have not been found in previous works. Yet, in addition to the comprehensive review presented relating to the use of the AC bus signaling concept, other contributions of this article are highlighted as follows:

- Present a fully decentralized control approach based on the integration of different droop-based strategies in which current- and voltage-controlled converters can be concomitantly steered within an autonomous MG to support efficient, reliable and safe operation;
- The proposed strategy allows to achieve proper power balance among GFCs, GSCs, and GFdCs at all times, ensuring adequate synergy among them. Such approach

TABLE 1. Summary of Literature Review Considering the Control of Autonomous MGs With Different Topologies of Converters.

Ref	Goal	Control Topology and Operation Mode of converters						Fully	Power Control		Overcurrent
		Principle	CCM	VCM	GFC	GSC	GFdC	Decent.	Active	Reactive	Control
[7]	Accurate reactive power sharing and compensation of voltage harmonics	Modified droop with capacitive virtual impedance Reverse droop control	✓	✓	✓	✗	✓	✓	✓	✓	✗
[22]	Power balance maintenance and charging control of BESSs with SoC equalization	Voltage-frequency bus signaling Conventional droop control	✓	✓	✓	✗	✓	✓	✓	✓	✗
[23]	Frequency regulation, and seamless transition between power-controlled and VCM modes	Frequency bus signaling Smooth switching droop control	✓	✓	✓	✗	✓	✓	✓	✓	✗
[24]	Frequency regulation, and prevention of overcharging and overdischarging in BESSs	Frequency bus signaling Primary and secondary layers	✓	✓	✓	✗	✓	✗	✓	✗	✗
[25]	Frequency regulation, power balance among RESs and BESSs, and prevention of overcharging in BESSs	Frequency bus signaling Virtual inertia loop Primary and secondary layers	✓	✓	✓	✗	✓	✗	✓	✗	✗
[26]	Frequency regulation and battery charging control	Frequency bus signaling Shifting-frequency droop term based on SoC of BESSs	✓	✓	✓	✗	✓	✓	✓	✗	✗
[28]	Frequency and voltage regulation, accurate reactive power sharing, and optimal active power control	Primary and secondary layers	✗	✓	✓	✗	✗	✗	✓	✓	✗
[29]	Frequency and voltage regulation, and battery charging control	Conventional droop control Battery voltage regulation with FBS.	✓	✓	✓	✗	✓	✓	✓	✓	✗
[30]	Active power control and mitigation of frequency deviation	Frequency bus signaling P-f droop using SoC of BESSs	✓	✓	✓	✗	✓	✓	✓	✗	✗
[31]	Real-time power balance under abnormal condition of short-term power shortage	Frequency bus signaling Constant-voltage constant-frequency control Classic droop control	✓	✓	✓	✗	✓	✓	✓	✓	✗
Here	Power balance maintenance, frequency and voltage regulation, prevention of overvoltage and overcurrent in BESS, and accurate power sharing	AC bus signaling Conventional droop control Modified droop control	✓	✓	✓	✓	✓	✓	✓	✓	✓

CCM stands for current-controlled mode, and VCM stands for voltage-controlled mode.

also provides means to automatically prioritize power generation from non-dispatchable RESs (e.g., PV-based generation). Additionally, concerning to the control of BESSs, both current- and voltage-controlled modes are supported, steering their converters without causing overvoltage or overcurrent of batteries, which improves the lifespan of such systems;

- As conventional droop control is inherently affected by mismatches in line impedances existing over the MG, a modified droop-based strategy, which is based on the voltage drop compensation of the line resistance in the voltage reference, is proposed to improve reactive power sharing accuracy and regulation of load bus voltage; its operational features are compared to a classic droop method.

It is also worth reinforcing that, with regard to the above-mentioned contributions and the work found in [32], this article: *i)* presents a different coordination approach for the converters, which uses different droop curves and limiting operational parameters; *ii)* incorporates the controllable overvoltage/overcurrent capabilities not previously discussed in [32]; and *iii)* brings more extensive literature review, as well as further discussions and simulation results to demonstrate the wide range of capabilities of the proposed methods.

Thus, this article is organized as follows. In Section II, the MG topology and decentralized operational premises are presented, demonstrating how active and reactive power are proposed to be regulated. In Section III, the control principles of current- and voltage-controlled converters are presented,

highlighting the droop-based schemes proposed for the GFC, GSC, and GFdC units to be considered. Simulation results are shown in Section IV comprising different operational conditions and scenarios to demonstrate the capabilities of the proposed integrated scheme. A summary of the findings of this article finally conclude the paper in Section V.

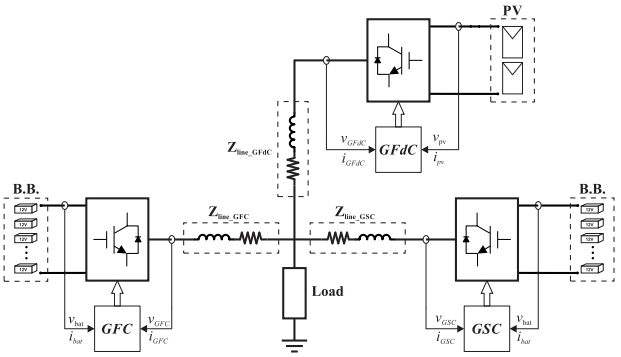

FIGURE 1. The considered autonomous decentralized MG structure.

II. STRUCTURE AND OPERATION OF AN AUTONOMOUS DECENTRALIZED MICROGRID

The considered MG topology adopted within this article, based on an autonomous perspective of operation, is shown in Fig 1. Such system is herein considered as a single-phase MG, and it basically comprises dispersed converters, which are driven according to different control perspectives under either current- or voltage-controlled modes, one generic load representing any consumer of electrical energy, as well as different line impedances among all point-of-couplings (PoCs). Note that converters are designed as either as PV-based generation or BESS, being this first implemented for the GFdC unit, and the latter considered for both the GFC and GSC units.

Since autonomous systems in general operate islanded, the GFC unit is endowed with the function of forming the AC grid, providing the voltage and frequency references to the whole MG. Thus, such converter is driven under a voltage-controlled approach, as a voltage source. On the other hand, the GFdC unit feeds the MG with the generated power from its primary energy source (i.e., its RES) [8]. Consequently, it runs as a controlled current source. Lastly, the GSC unit is capable of absorbing or injecting active and reactive power to support the MG's voltage and frequency regulation. Due to its flexibility of operation, such unit might be steered as either a controlled voltage source or a controlled current source, depending on the desired operational behavior.

Regarding the MG infrastructure and its operational aspects, the following additional considerations are important to be highlighted: *i)* the MG operation dynamics is determined by the GFC unit, since this converter imposes the voltage amplitude (V) and angular frequency (ω) for the entire system; *ii)* the GSC and GFdC units operate responding to the variations of (V) and (ω), adjusting their active and reactive powers accordingly; and *iii)* the AC bus signaling principle and droop-controllers regulate the active and reactive power processed by the converters, being described as follows.

A. ACTIVE POWER SHARING

When BESSs exist within a MG, there are two crucial operational aspects that need to be accounted for maintaining the integrity and ensuring long lifespan of such storage elements. The first aspect is to keep the magnitude of the recharge current of a BESS below its designed maximum limit. With respect to the second aspect, it is required to maintain the terminal voltage of the batteries within acceptable range, avoiding overvoltage stresses. Taken together, these two aspects also need to be accounted for the steering of the GFC unit, beyond their employment on imposing adequate voltage and frequency signals, dictating proper transient and steady-state dynamics for the entire MG.

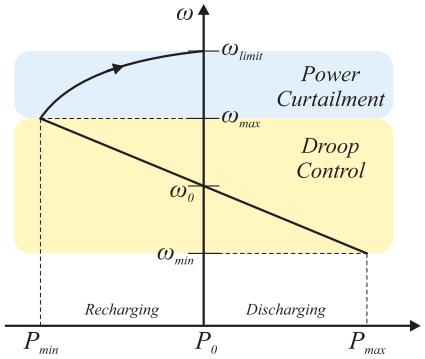

FIGURE 2. $P-\omega$ droop curve with power curtailment for GFC and GSC units.

The operational principle and active power (P) balance of the GFC unit is presented in Fig. 2, its relationship with the MG angular frequency can be identified. There are two regions that establish the operational range of the system. The first region, called "Droop Control", sets the normal condition of the MG, and the GFC unit injects or absorbs active power without controlling the recharging current or voltage of its battery bank. For such scenario, when the power drawn by the loads is greater than the power supplied by the RESs, power contribution from the batteries is required. Thus, the GFC unit decreases the grid frequency proportionally to the supplied active power, as seen in Fig. 2.

The droop curve of Fig. 2 is implemented in the GFC unit, which determines the MG frequency dynamics. Thus, whenever the GFC provides or absorbs active power, the MG frequency varies from its rated value (ω_0), but being always within a predetermined range (ω_{min} and ω_{max}). The adopted frequency range is set on the basis of the allowed frequency excursion given in accordance with the international standard CENELEC EN50160 [33], which defines a frequency variation of $\pm 2\%$ for isolated systems not fed by synchronous generators, as described in Section III-A.

On the contrary, when the power provided by RESs is greater than the loads demand, the surplus energy must recharge the battery banks spread over the MG. Under such condition, the GFC increases the grid frequency to share the remaining power among the battery banks of GFC and GSC units, in accordance with their droop equations. Thus, both converters endowing BESSs are able to provide power to the MG and to be recharged proportionally to their rated powers. On the other hand, in respect to the second region of operation given in Fig. 2, namely "Power Curtailment", if the active power supplied by the RESs is excessively high, the recharging current of the GFC's battery system may exceed its maximum value and such a parameter must therefore be limited. To achieve such functionality, the MG frequency is increased to an operation point between the range of ω_{max} and ω_{limit}.

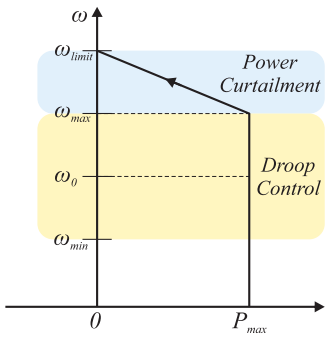

FIGURE 3. $P - \omega$ droop curve with power curtailment for the GFdC unit.

For the GFdC units, as seen in Fig. 3, active power conversion is provided as much as possible, according to the maximum power point tracking (MPPT) setpoint, when at nominal frequency (ω_0) and when within normal operational condition. Simultaneously, as shown in Fig. 2, when ω_0, the GFC and GSC units do not provide active power, ensuring that the use of power from non-dispachable renewable sources (i.e., such as the PV-based one) take precedence over the dispatchable ones (i.e., BESSs), unless power insufficiency occurs from high load consumption. In respect to the power curtailment region, Fig. 3 demonstrates that the GFdC unit is controlled to constrain its output power if the MG frequency is higher than ω_{max}, up to the point of presenting null generation if the frequency deviates above ω_{limit}.

Another scenario existing within the power curtailment region of Figs. 2 and Fig. 3 is the voltage control of the GFC's battery bank, which follows the same aforementioned strategy for limiting the recharge current. By reaching the maximum allowed voltage of its battery bank, also known as gasification voltage, the GFC unit increases the frequency to a value between ω_{max} and ω_{limit} to curtail the power supplied by the GFdC one, aiming at keeping the terminal voltage of its battery bank constant, while still presenting lower recharging current.

Finally, in regard to the GSC unit, its operational active power curve resembles the $P - \omega$ droop region presented in Fig. 2. Such converter follows a current-controlled approach, consequently constraining its maximum recharging current and limiting its voltage value as required to avoid operation above nominal values. Additionally, the converter independently stops the recharging process when the battery is fully-recharged, ensuring that the two before-mentioned crucial operational aspects for battery-based converters are obeyed.

B. REACTIVE POWER SHARING

This paper considers the relationship between $P - \omega$ and $Q - V$ as control premises; hence, the voltage amplitude of the MG corresponds to reactive power (Q) flow control. Besides, under an autonomous perspective of operation, it is intended that the reactive power demanded by loads should be proportionally shared among the dispersed converters. Nonetheless, when adopting classic droop control technique, the inaccuracy of reactive power sharing among DERs is commonly caused by line impedance mismatching alone or together with different droop gains among converters [34].

Consequently, in this article, the RMS voltage acts as bus signaling for current-controlled converters to provide the correct amount of reactive power. However, when different line impedances between the converters and the load (i.e., main bus) exist, the RMS voltage value at each converter is different if compared to other PoCs due to the voltage drop in the impedances. This situation causes the current-controlled converters to measure RMS voltage values different from the MG rated value, and thus to obtain inaccurate values of reactive power. As a result, this causes high current flow among converters when the MG operates without load demand, also impairing reactive power sharing performance. For the case of two converters comprising the same rated power, for example, the one with lower impedance provides the largest portion of reactive power. Then, to minimize the influence of line impedance in reactive power sharing, this article proposes a new and modified droop equation (1) that compensates the voltage drop of line resistance, adding its value ($R_{line} \cdot I_{active}$) to the voltage reference.

$$V = (V_0 + R_{line} \cdot I_{active}) - k_n \cdot (Q - Q_0) \tag{1}$$

Similar approaches were proposed in [34]–[36], in which the voltage drop in the virtual resistance is subtracted from the voltage reference used for the converter control. Nevertheless, unlike these studies, one proposes to add the voltage drop to the voltage reference, which inherently also provides improved voltage regulation at the load bus.

In general, the value of the line resistance (R_{line}) is estimated knowing the distance between the PoC of a converter and the neighbouring circuit node, as well as the cable parameters to be used for the connection. However, for MGs with several distributed loads, the line impedance value is different for each load; in these cases, rendering this technique as less effective. Nonetheless, this aspect does not affect the small-scale MG topology considered within this article.

This article considers the implementation of the GFdC unit also contributing to reactive power sharing, according

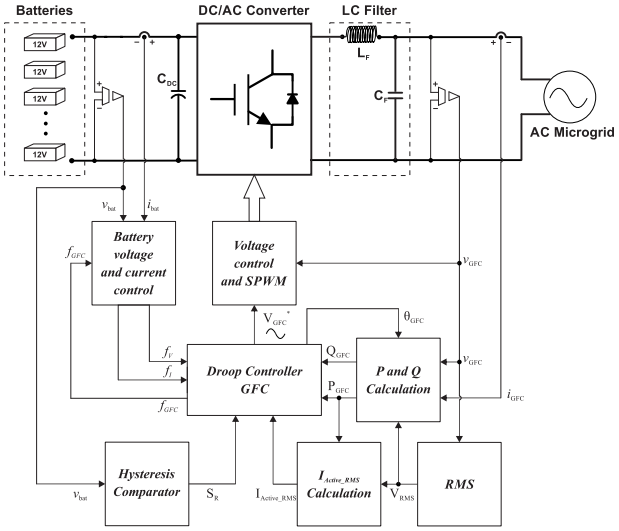

FIGURE 4. Block diagram of structure and control scheme of GFC.

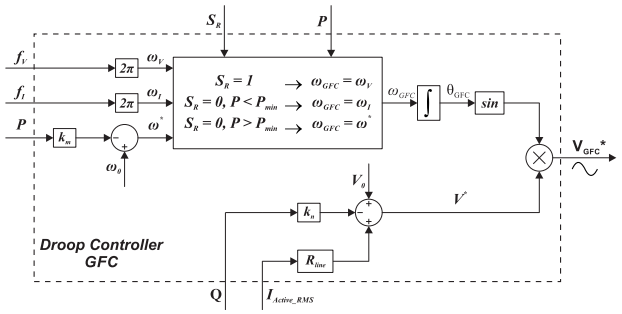

FIGURE 5. Block diagram of GFC Droop Controller.

to (1). Therefore, the reactive power is more adequately and proportionally divided among GFC, GFdC, and GSC units, than when conventional droop is employed. The following section will further explain the implementation process of the aforementioned active and reactive power control schemes, for all three converter topologies.

III. CURRENT AND VOLTAGE CONTROL SCHEMES FOR CONVERTERS IN A DECENTRALIZED MG

A. GRID-FORMING CONVERTER

The GFC unit is responsible for imposing the voltage and frequency AC signals for the entire MG operation. Fig. 4 shows the power electronics structure and control scheme of GFC. As illustrated, there are two main blocks in the control structure of this converter: the ''Droop Controller GFC'' block and the ''Battery voltage and current control'' block. The remaining control structure of this converter is a classic grid-forming converter, in which the ''Voltage control and SPWM'' block presents inner voltage/current control loops [8] and the sinusoidal PWM modulator that generates the command to the power switches.

1) DROOP CONTROLLER OF THE GFC UNIT

The main feature of this block is the implementation of the droop controller. It is used to generate the voltage reference for the voltage-controlled operation of the GFC, to adequately control the voltage magnitude and frequency of the MG. A summary of the implementation of this droop-based approach for the GFC unit is shown in Fig. 5.

In such control structure, once the GFC operates in the ''Power curtailment'' region, the ''Hysteresis Comparator'' block provides the S_R signal to the GFC Droop Controller, which indicates the need for power curtailment according to the voltage value of the battery bank (v_{bat}). Then, (v_{bat}) is measured and, if such quantity is above V_{batmax}, which is the gasification voltage value of this system, then the Hysteresis Comparator sets $S_R = 1$. Under such condition, the GFC Droop Controller block takes its f_v input, which is the frequency provided by the Voltage Controller of the battery, and multiplies it by 2π to obtain a value between ω_{max} and ω_{limit}, resulting in $\omega_{GFC} = \omega_V$. Thus, when the GFC unit provides active power and the V_{bat} voltage leaves the hysteresis loop (i.e., reducing its value to less than $V_{batmax} - \Delta V$), the signaling value is $S_R = 0$. In such a case, the value of $V_{batmax} - \Delta V$ gives the voltage value of the battery bank in a fully charged open circuit.

When maximum battery current is reached during recharging, a minimum power P_{min} according to the desired maximum recharge current and battery voltage must be defined. Thus, by reaching an active power value inferior to P_{min}, the frequency used for the reference voltage is replaced by ω_I, provided by the battery current controller (i.e., $\omega_{GFC} = \omega_I$), in such a way that the GFdC unit limits its generated power and consequently reduces the battery recharging current.

When there is no need for power curtailment, the frequency is defined by (2), which comes from the classic $P - \omega$ droop law, characterizing the GFC operation within the ''Droop Control'' region of Fig. 2, having $\omega_{GFC} = \omega^*$. Additionally, for the GFC unit to reach the adequate peak voltage value (V^*) (i.e., voltage magnitude) at its output, (3) is used, originated from (1), but considering $Q_0 = 0$.

$$\omega^* = \omega_0 - k_m \cdot P \tag{2}$$

$$V^* = (V_0 + R_{line} \cdot I_{active}) - k_n \cdot Q \tag{3}$$

The coefficients k_m and k_n in Fig. 5 are calculated as (4) and (5):

$$k_m = \frac{\omega_{max} - \omega_{min}}{P_{max} - P_{min}} \tag{4}$$

$$k_n = \frac{V_{max} - V_{min}}{Q_{max} - Q_{min}} \tag{5}$$

The ω_{max} and ω_{min} quantities define frequency variation according to the active power of the GFC unit. On the other hand, V_{max} and V_{min} define the variation of voltage amplitude as a function of the reactive power. Herein, the k_m and k_n coefficients are set on the basis of the allowed frequency excursion given in accordance with the international standard CENELEC EN50160 [33] and by following the Brazilian

TABLE 2. Limit Values for Frequency and Voltage Variation.

Parameter	Value
ω_0	377 [rad/s]
ω_{min}	373.23 [rad/s]
ω_{max}	380.77 [rad/s]
ω_{limit}	384.54 [rad/s]
V_0	311.13 [V]
V_{min}	295.57 [V]
V_{max}	326.68 [V]

ANEEL Normative Resolution 469 [37]. It is defined a frequency variation of $\pm 2\%$ for isolated systems not fed by synchronous generators and voltage variation limits of 202 Vrms to 231 Vrms (i.e., for nominal 220 Vrms at 60 Hz).

In summary, the GFC unit operates in two regions (i.e., the "Droop Control" and the "Power curtailment"), with four ranges of frequency values. Frequency is found in $\pm 1\%$ for this first region, and in $+2\%$ for the latter one, with a nominal frequency of 60 Hz. Similarly, the voltage may vary in 5%, with respect to the nominal peak voltage of 311 V (i.e., 220 Vrms). Such values are gathered in Table 2, showing the allowed limits set for frequencies and voltages.

Finally, the control scheme of the GFC unit is concluded by taking the ω_{GFC} and integrating it to generate the θ_{GFC} angle of the converter reference voltage. Later, such signal feeds a sine function and the output is multiplied by the peak value V^*. Therefore, a sinusoidal voltage is generated by the converter with frequency ω_{GFC} and amplitude V^*.

2) GFC BATTERY VOLTAGE AND CURRENT CONTROLS

The second most important control block of the GFC unit (i.e., "Battery voltage and current control" functions) is expanded in Fig. 6. Such block diagrams represent the means to provide frequency values to synthesize the reference voltage for the converter, aiming at maintaining a maximum value of voltage or current during the battery recharge procedure. The battery voltage and current controllers are split to facilitate the understanding.

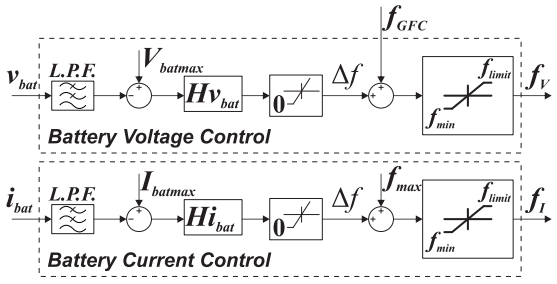

FIGURE 6. Block diagram of battery voltage and current control loops for the GFC unit.

The proposed voltage control scheme in Fig. 6 provides a frequency signal (f_v) to be synthesized by the converter, considering that such frequency value is useful to automatically and indirectly steer the GFdC unit so that it can reduce its output power when needed. This signal prompts the regulation of the recharge current of the battery bank, consequently maintaining a fixed terminal voltage value (V_{batmax}). To curtail the output power of the GFdC unit, the value of the output frequency (f_v) of this control must be within the limit f_{max} and f_{limit}. Thereby, the current frequency of the GFC unit is added to the Δf value, and a limiter is employed on the control output for reassurance. Since the frequency varies depending on the battery voltage, a low-pass filter (LPF) is used to filter out the voltage fluctuation, thus obtaining an average voltage value and offering reduced frequency oscillations.

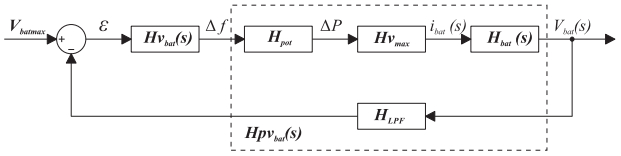

FIGURE 7. Block diagram of battery voltage control scheme of GFC.

The Hv_{bat} controller is tuned based on the system model represented in Fig. 7. Besides, the Hpv_{bat} plant seen by the controller is composed by the battery bank (H_{bat}), the Hv_{max} gain, the H_{pot} transfer function, and the LPF transfer function (H_{LPF}). The term H_{pot}, given by (6), represents the amount of power that will be reduced according to the obtained frequency variation. The power variation on the GFdC unit is linear with respect to frequency variation. Therefore, H_{pot} is modeled as a static gain calculated as the inverse of k_m, with opposite sign due to the control action.

The Hv_{max} gain converts power into current to recharge the battery. Considering that, during the action of the control, the battery terminal voltage varies around V_{batmax}, the term (7) is obtained. The H_{bat} transfer function, which represents the physical modeling of the battery bank, is derived from the the model for lead-acid batteries proposed in [38]. Such formulation is based on a Thevenin equivalent circuit and results in a transfer function that relates the terminal voltage of the battery bank with the current. Consequently, the entire circuit is considered as an equivalent impedance and is given by (8). To extract the average component of the battery terminal voltage, a second-order LPF is used, as shown in (9). Moreover, the battery voltage presents ripple, due to the switching of the GFC converter, which has an oscillatory component at 120 Hz. Therefore, the LPF is tuned to a cut-off frequency of $\omega_c = 10\ Hz$, using a damping coefficient of $\xi = 0.707$.

Thus, the open-loop transfer function is obtained by (10), being represented by Fig. 7. Finally, to define the parameters of the Hv_{bat} controller, it is set a cut-off frequency for the compensated open-loop system of 10 times the cut-off frequency of H_{bat}, which has the slowest and most predominant dynamics of the plant. Therefore, $f_{c_{OL_{Vbat}}} = 10 \times f_{c_{H_{bat}}}$. Then, based on a frequency design method [39], it is possible to calculate the parameters of the controller. The module of the compensated open-loop system at the cut-off frequency is

unity and the phase margin (PM) is set close to 60°.

$$H_{pot} = -\frac{1}{k_m} = \frac{P_{min} - P_0}{f_{limit} - f_{max}} \tag{6}$$

$$Hv_{max} = \frac{1}{V_{batmax}} \tag{7}$$

$$H_{bat}(s) = \frac{v_{bat}}{i_{bat}} = \left(\frac{1}{s \cdot C_0} + R_s + \frac{R_1}{s \cdot C_1 \cdot R_1 + 1}\right) \tag{8}$$

$$H_{LPF}(s) = \frac{\omega_c^2}{s^2 + 2\xi\omega_c \cdot s + \omega_c^2} \tag{9}$$

$$OL_{Vbat}(s) = Hv_{bat}(s) \cdot H_{pot} \cdot Hv_{max} \cdot H_{bat}(s) \cdot H_{LPF}(s) \tag{10}$$

Now, likewise done for the voltage controller, the battery current control scheme is devised as shown in Fig. 6. When the battery recharging current reaches a value higher than the previous defined threshold I_{batmax}, the controller Hi_{bat} varies the frequency that is added to the f_{max}. Consequently, power curtailment occurs at the output of the GFdC unit, guaranteeing a constant value of recharging current.

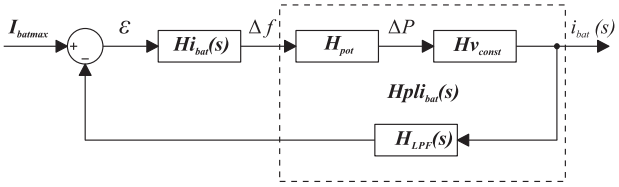

FIGURE 8. Block diagram of battery current control scheme for GFC.

To tune the Hi_{bat} controller consider the system shown in Fig. 8. Hence, the $Hpli_{bat}$ transfer function seen from the controller comprises the H_{pot} gain, the Hv_{const} gain, as well as the LPF transfer function H_{LPF}, used to obtain the average from the current signal that may present oscillations of 120 Hz.

For such current control scheme, the same H_{pot} function of (6) is used. As the dynamics of the current signal is much faster than the battery voltage V_{bat}, the latter is considered constant from the current control perspective. Thus, the Hv_{const} gain resembles (7), but the value of the nominal voltage (i.e., 12 V) for each battery is used, as represented by (11). The LPF function is the same as before for (9).

$$Hv_{const} = \frac{1}{V_{const}} \tag{11}$$

Using a PI controller for Hi_{bat}, the open-loop transfer function is found for the battery current control, as in (12). It is important to highlight that the dynamics of the control plant are dominated by the features of the LPF design. Therefore, to calculate the parameters of the controller, a cut-off frequency for OL_{Ibat} is chosen, to be close to the cut-off frequency of H_{LPF}, which is 10 Hz.

$$OL_{Ibat}(s) = Hi_{bat}(s) \cdot H_{pot} \cdot Hv_{const} \cdot H_{LPF}(s) \tag{12}$$

B. GRID-FEEDING CONVERTER

This section details the structure and control scheme of the GFdC unit presented in Fig. 9. The "PLL" block detects the

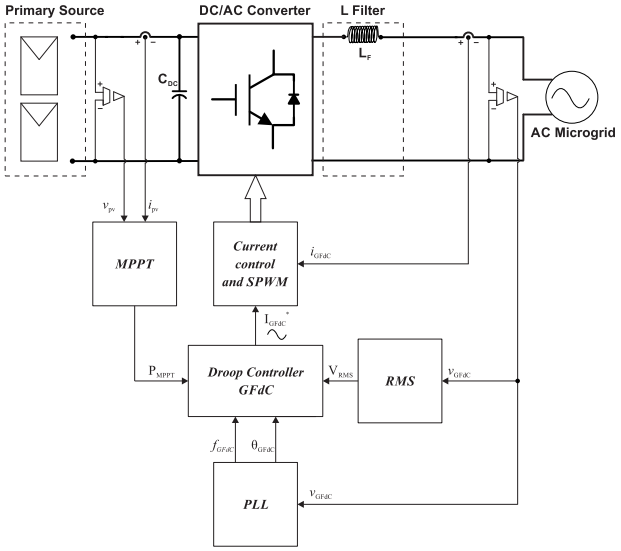

FIGURE 9. Block diagram of structure and control scheme of the GFdC unit.

frequency and voltage angle of the PoC for the converter to operate under current-controlled mode, also used for the synchronization algorithm. A simplified single-phase PLL algorithm is used, as described in [40]. The "Current control and SPWM" block represents the inner current control loop and sinusoidal PWM modulator that drives the power switches of the converter. Yet, the "MPPT" block comprises the tracking algorithm of maximum power point of the primary energy source. As previously mentioned, the current-controlled operation of the GFdC also relies on a droop controller, explained in the following section.

1) GFdC DROOP CONTROLLER

Fig. 10 expands the "GFdC Droop Controller" block that is responsible for providing the AC current reference $I_{GFdC}{}^*$ for the converter. This reference is attained based on the frequency f_{GFdC} and voltage V_{RMS} quantities sensed at that PoC. The $I_{GFdC}{}^*$ current signal is synthesized by the sum of two quantities, the active (I_{Active}) and reactive ($I_{Reactive}$) current components. This first component (i.e., I_{Active}) is obtained by dividing the active power P_{GFdC} by the measured V_{RMS} voltage. Sequentially, the magnitude of the current component is obtained and synchronized with the MG voltage by multiplying it by the $sin(\theta_{GFdC})$ function, obtained from the PLL.

Again, the active power (P_{GFdC}) is defined under two regions of operation: the "droop control" and the "power curtailment", as shown in Fig. 3, and as ruled by the frequency f_{GFdC} attained in respect to the AC voltage signaling from that PoC. Once operation occurs in the "droop control" region, power curtailment does not occur, since the battery bank of the GFC unit is not fully recharged. Consequently, f_{GFdC} must be lower than f_{max}, steering the GFdC unit to convert the maximum power available at its DC side, so that the power

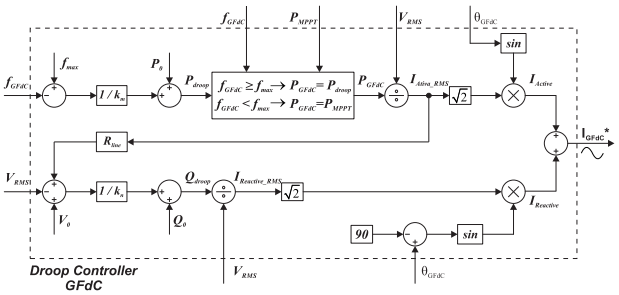

FIGURE 10. Block diagram of droop controller for the GFdC unit.

from its renewable source (P_{MPPT}) is fully exploited on the basis of the MPPT algorithm.

Under a operational condition within the ''power curtailment'' region, the f_{GFdC} frequency becomes greater than, or equal to f_{max}, which leads to $P_{GFdC} = P_{droop}$. In this case, P_{droop} is the power reference in response to frequency variation. For this GFdC unit, the droop equation for active power control is given by (13), in which P_0 is the nominal power of the primary energy source, and k_m is the slope coefficient calculated by (14). The term P_{min} is considered null, since the considered GFdC unit does not absorb power, and P_{max} is the converter rated power.

$$P_{droop} = P_0 + \frac{f_{max} - f_{GFdC}}{k_m} \tag{13}$$

$$k_m = \frac{f_{limit} - f_{max}}{P_{max} - P_{min}} \tag{14}$$

With regard to the reactive current component, $I_{Reactive}$, it is obtained by dividing the reactive power Q_{droop} by the PoC voltage V_{RMS}, later synchronized with the quadrature component of the voltage by being multiplied by $sin(\theta_{GFdC} - 90)$. Q_{droop} is derived from (1) and rearranged in (15). Yet, in such formulation, Q_0 is the reactive power set by a secondary controller, considered null since this control layer does not exist in the fully decentralized scheme within this article. The term $R_{line} \cdot I_{active}$ in (15) is the voltage drop on the estimated line resistance on the GFdC side, and kn is calculated as in (5).

$$Q_{droop} = Q_0 + \frac{V_0 + R_{line} \cdot I_{active} - V_{RMS}}{k_n} \tag{15}$$

C. GRID-SUPPORTING CONVERTER

The GSC unit is also a converter powered by a battery bank at its DC side, similar to the topology of the GFC unit, although endowed with output current control (i.e., as it is here operated under current-controlled mode). Fig. 11 shows the structure and control scheme of this GSC unit. Due to the nature of operation of this converter, the output current i_{GSC} should accurately follow the reference current $I_{GSC}{}^*$. Then, the ''GSC Droop Controller'' block is responsible for providing the current reference $I_{GSC}{}^*$, while the ''Battery voltage control'' block is needed to regulate the maximum battery voltage. Both control blocks are detailed in the following section.

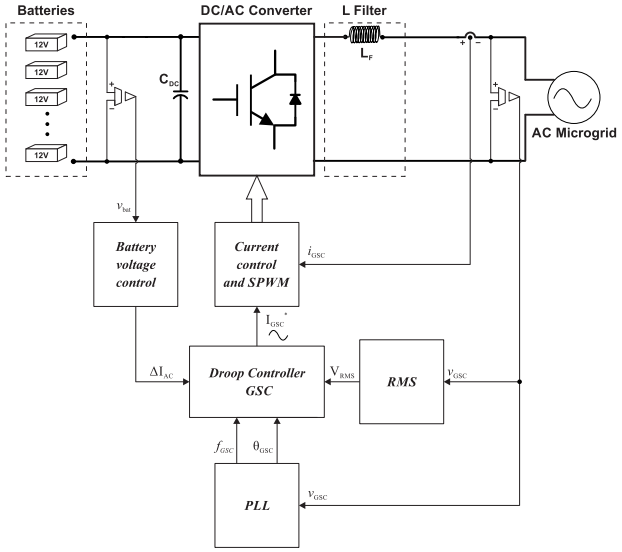

FIGURE 11. Block diagram of structure and control scheme of the GSC unit.

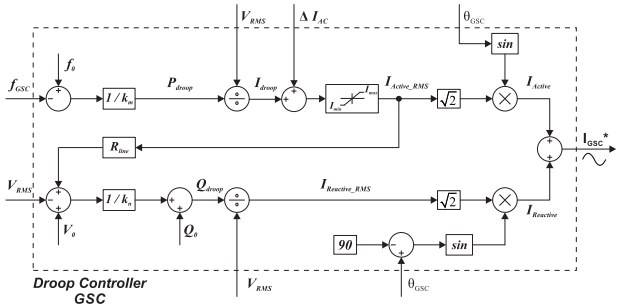

FIGURE 12. Block diagram of Droop Controller for GSC.

1) DROOP CONTROLLER FOR THE GSC UNIT

This block provides the current reference used within the inner current control loop, represented by the ''Current control and SPWM'' block in Fig. 11. Fig. 12 shows how the $I_{GSC}{}^*$ current is defined. Such structure resembles the droop dontroller of the GFdC unit, since both are operating under current-controlled mode. Therefore, analogous to the grid-feeding converter, the $I_{GSC}{}^*$ current for the GSC unit is split into two terms, which are I_{Active} and $I_{Reactive}$.

The calculation of the reactive current term is identical to the approach used for the GFdC unit. On the other hand, for the calculation of the active current term, the P_{droop} term in (16) is computed first, later converted to current for the GSC control. The k_m coefficient is calculated as in (4).

$$P_{droop} = \frac{(f_0 - f_{GSC})}{k_m} \tag{16}$$

Then, P_{droop} is divided by the PoC voltage (V_{RMS}), resulting in I_{droop}, which is later added with the outcome of the ''Battery Voltage Control'' block (ΔI_{AC}). When I_{droop} is negative, the battery voltage reaches its maximum value. Consequently, the ''Battery voltage control'' block provides a ΔI_{AC} value that, when added to the negative value of

I_{droop}, the absolute value of I_{Active_RMS} is reduced. Therefore, the battery recharging current is limited and its terminal voltage is kept controlled at a constant value. If $v_{bat} < V_{batmax}$, then the ΔI_{AC} value is null. Moreover, since the GSC unit operates under current-controlled mode, a maximum battery current regulator is not needed, as it is enough to add an internal limiter to the output current.

2) BATTERY VOLTAGE CONTROL FOR THE GSC UNIT

Similar to the GFC, the voltage of the battery bank of the GSC unit needs to be controlled, which is achieved by regulating the value of the AC current reference of the GSC. A summarized scheme of this strategy is shown in Fig. 13.

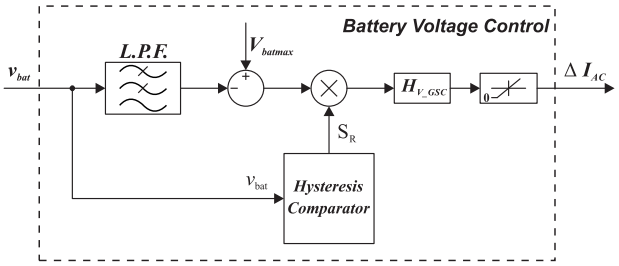

FIGURE 13. Block diagram of battery voltage control for the GSC unit.

The battery average voltage is obtained through a LPF, as done for the GFC unit, and compared to a maximum voltage value (V_{batmax}) established. The error goes through the H_{V_GSC} controller, and ΔI_{AC} feeds the "GSC Droop Controller" block. The error is, beforehand, multiplied by the S_R signal of the "Hysteresis comparator" block in Fig. 13, which establishes $S_R = 1$ only when the v_{bat} voltage exceeds the V_{batmax} threshold, analogously to the GFC unit.

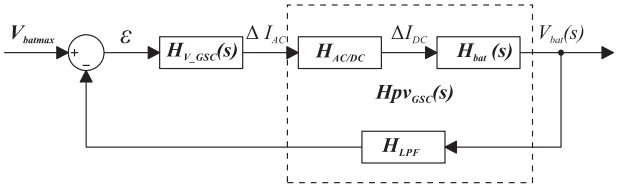

FIGURE 14. Battery voltage control model for designing the H_{V_GSC} controller.

For the design of the H_{V_GSC} controller, the system model shown in Fig. 14 is considered. The Hpv_{GSC} plant used for the design of the controller is composed of the battery bank H_{bat}, using the same design principle as in (8), the $H_{AC/DC}$ gain, which converts the AC current reference to the battery DC current, and the LPF as in (9). To calculate the $H_{AC/DC}$ gain, an ideal system with no-losses must be considered, and constant battery voltage is obtained by the controllers' action. Therefore, the DC power will be equal to the AC power, but with opposite signs, due to the direction of the adopted polarity. Thus, the ratio between I_{DC} and I_{AC} is obtained by (17). Finally, for tuning the H_{V_GSC} controller, the same methodology adopted for the battery voltage control of the GFC unit is used, as long as a cut-off frequency for the compensated open-loop system is 10 times higher than the cut-off frequency of H_{bat}.

$$H_{AC/DC} = \frac{I_{DC}}{I_{AC}} = -\frac{V_{RMS}}{V_{batmax}} \tag{17}$$

IV. SIMULATION RESULTS

The autonomous MG topology presented in Fig. 1 was implemented by means of the PSIM sofware, used as a testbench for simulation results, to demonstrate the operation features of the proposed decentralized strategy of the current- and voltage-controlled converters (i.e., one GFC unit, one GFdC unit, and one GSC unit). In a MG with more than one GSC or GFdC, the converters would still share active and reactive power proportionally to their rated power, and it is reinforced that the control approach would have the same performance, without impacting the overall operation herein demonstrated. Such a scenario has been reported in [41]. The existing load is implemented to assume variable behaviors and values depending on the case study targeted. For instance, firstly, the simulated cases are considered only the presence of resistive loads, and later on further results considered RL loads. Moreover, the controllers proposed and designed throughout the paper are concomitantly verified herein.

Five simulation scenarios are presented to assess the main features of the proposed control methods, in which it is demonstrated that: *A)* active power injection generated from RESs is prioritized over generation from dispatchable sources (i.e., BESSs); *B)* battery-based converters support the injection of active power if RESs are not able to properly supply the loads; *C)* batteries are recharged proportionally among converters comprising such systems, according to their rated power, regardless of their control topology; *D)* power curtailment is adequately performed to avoid overvoltage/overcurrents in BESSs; and *E)* the modified droop control proposed for reactive power sharing is presented and compared with classic droop control.

In this article, it is considered PV-based generation for the GFdC, and BESS for the GFC and GSC units, but other sources could also be used (e.g., wind turbines or microturbines). As wind turbines are not dispatchable sources and use MPPT algorithms, they would fit within the same approach as the one for PV sources, controlled as GFdC. Micro-turbines, on the other hand, are dispatchable sources that do not store energy. Consequently, they could be considered as a GSC with null minimum active power ($P_{min} = 0$) for calculating the k_m coefficient in (4) and (16). By doing so, they would adequately perform proper power sharing with other converters. Another slight difference in the control scheme would be the absence of the "Battery voltage control" block, which would not impair the system performance.

The considered parameters of the battery models are presented in Table 3, being based on [38]. For the GFC unit, a bank with 34 lead-acid batteries is considered, presenting nominal capacity of 220 Ah. For the GSC unit, the same

TABLE 3. Battery Banks Equivalent Circuit Parameters.

GFC battery bank parameters			
$\mathbf{C_0}$ (F)	$\mathbf{C_1}$ (F)	$\mathbf{R_1}$ (Ω)	$\mathbf{R_S}$ $(m\Omega)$
10588.25	14	2	85
GSC battery bank parameters			
$\mathbf{C_0}$ (F)	$\mathbf{C_1}$ (F)	$\mathbf{R_1}$ (Ω)	$\mathbf{R_S}$ $(m\Omega)$
3032.09	4.01	6.99	170

TABLE 4. Simulation Parameters of GFC, GFdC and GSC.

GFC Simulation Parameters	Value
Rated power (S_{GFC})	22500 VA
Output voltage (V_{AC})	220 V
L_F inductor	0.6 mH
C_F capacitor	7.6 μF
Switching frequency (f_s)	15 kHz
Power P_{max} | P_{min}	18000 | -18000 W
Power Q_{max} | Q_{min}	13500 | -13500 var
Max. battery voltage (V_{batmax})	476 V
Max. battery current (I_{batmax})	44 A
Z_{line_GFC}	$0.071 + j0.017\ \Omega$
GFdC Simulation Parameters	**Value**
Rated power (S_{GFdC})	31250 VA
L_F inductor	0.33 mH
Switching frequency (f_s)	15 kHz
Power P_{max} | P_{min}	25000 | 0 W
Power Q_{max} | Q_{min}	18750 | -18750 var
Z_{line_GFdC}	$0.047 + j0.011\ \Omega$
GSC Simulation Parameters	**Value**
Rated power (S_{GSC})	6250 VA
L_F inductor	4 mH
Switching frequency (f_s)	15kHz
Power P_{max} | P_{min}	5000 | -5000 W
Power Q_{max} | Q_{min}	3750 | -3750 var
%hline Max. battery voltage (V_{batmax})	476 V
Max. battery current (I_{batmax})	12.25 A
Z_{line_GSC}	$0.277 + j0.009\ \Omega$

arrangement of 34 batteries of 12V in series is considered, however, with batteries of 63 Ah of nominal capacity. The parameters of the GFC, GFdC and GSC units are shown in Table 4. The values for voltage and frequency variations of the MG are in Table 2.

A. ACTIVE POWER PRIORITIZATION FROM RES

The results of this first simulated case study are shown in Fig. 15, in which the MG initially presents no load and a load step occurs at 1.5 s. The load power is considered to be equivalent to the RES available power (i.e., the power being generated by the GFdC unit). The power supplied by the RES is automatically prioritized in relation to the power provided by batteries-based converters. This is certified by the fact that only the GFdC unit provides active power, while the GFC and GSC units operate standing by (i.e., practically not processing active power). The grid frequency is adequately regulated to its nominal value of 60 Hz, showing adequate synergy among the converters.

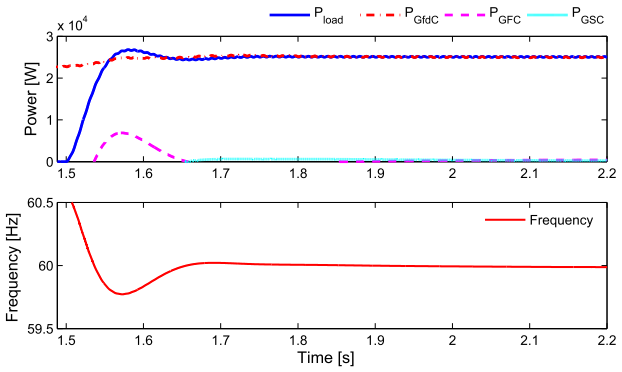

FIGURE 15. Case study 1 - RES generation taking precedence over BESSs.

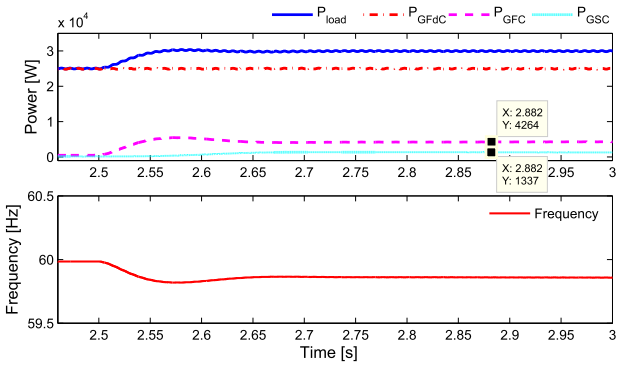

FIGURE 16. Case study 2 - Distributed batteries contributing proportionally to active power provision.

B. EXPLOITATION OF BESS FOR POWER CONTRIBUTION

This second scenario is a continuation of the previous result, demanding an additional load step to occur at 2.5 s, as seen in the result depicted in Fig. 16. For such condition, the load demanded power becomes higher than the RES available power. Thus, the battery-based converters contribute with power proportionately to their nominal ratings. It is demonstrated that, in 2.88 s, the GFC and the GSC units provide approximately 25% of their nominal powers. Consequently, in Fig. 16 the RES is prioritized, as the GFdC unit keeps processing its maximum power available and the other converters increase their active power injection. Additionally, this feature is possible due to the fact that the frequency is below the pre-set value limit of 60.6 Hz (f_{max}).

C. PROPORTIONAL RECHARGE OF DISTRIBUTED BESS

The case study 3 represented in Fig. 17 considers a load power inferior to the available power from the GFdC unit. Under such conditions, the extra power of the GFdC unit recharges the batteries of the GFC and GSC units, which occurs proportionally to their rated powers, and aims to maintain power balance. Note in Fig. 17 that the GFC and GSC units are recharged proportionally and steadily with approximately 82% of their minimum powers at 2.07 s. In addition, practically no significant frequency deviation occurs during such operation.

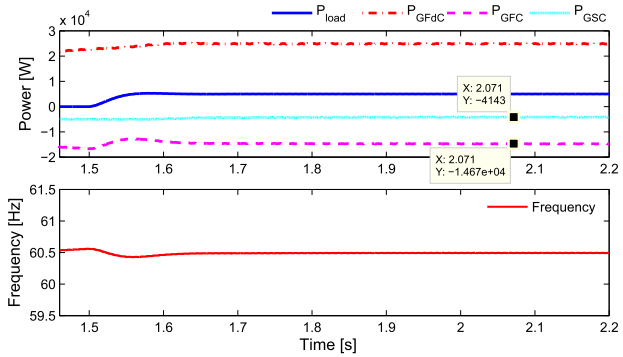

FIGURE 17. Case study 3 - proportional recharge of distributed battery banks.

D. OPERATION UNDER RES POWER CURTAILMENT

For this scenario, two simulated case studies demonstrate the possible conditions to cause active power curtailment from RESs, characterized by reaching the maximum voltage or maximum current of the battery system of the GFC unit. Thus, both conditions need to be properly addressed by the employed controllers.

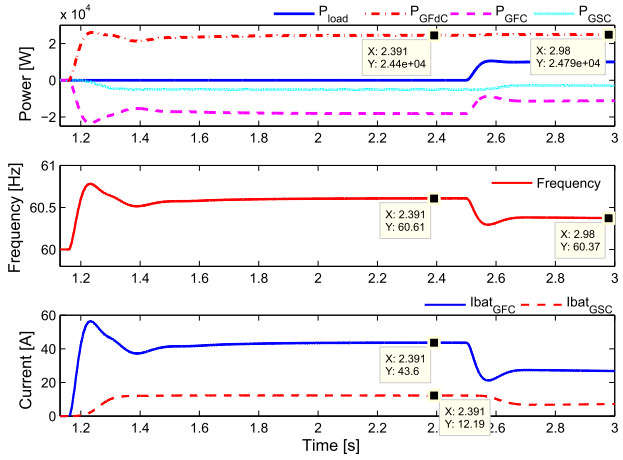

FIGURE 18. Case study 4 - RES power curtailment due to maximum current of GFC battery.

1) MAXIMUM CURRENT CONTROL OF THE GFC BESS

Firstly, case study 4 shown in Fig. 18 considers the MG operating without loads, while having the maximum power from the GFdC unit (i.e., the one comprising RES) available for charging the batteries of the GFC and GSC units. In steady state, the average current of the GFC BESS tends to exceed its maximum limit, which is $I_{batmax} = 44\ A$. Thus, the "Battery current control" block of the GFC unit increases the grid frequency to a value greater than f_{max}, so that the GFdC unit automatically curtails its output power. This condition characterizes the system operation as on the "Power curtailment" region of the control curves previously explained in Sections II and III.

By analyzing Fig. 18 it is possible to note that the frequency is 60.61 Hz at 2.39 s (i.e., it is above the maximum limit of 60.6 Hz), consequently leading the GFdC unit to curtail its output power to 24.4 kW. Such integrated condition imposed by the decentralized control approach allows for the limitation of the recharge current of the GFC unit to 43.6 A, which is below $I_{batmax} = 44\ A$. Moreover, it can be seen that the GSC unit performs its own current regulation, in an autonomous manner, absorbing a maximum current 12.19 A.

Later in this simulated case, a load step occurs at 2.5 s, causing the battery to reduce its recharging current, and consequently, triggering the GFC unit to lower its frequency value to 60.37 Hz, returning the MG operation to the "Droop Control" region. Besides, the GFdC unit is steered to provide its maximum available power of 2479 kW.

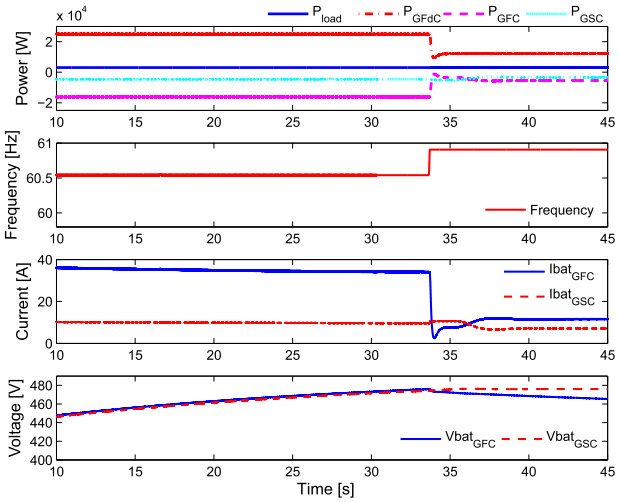

FIGURE 19. Case study 5 - RES power curtailment due to maximum voltage of GFC battery.

2) MAXIMUM VOLTAGE CONTROL OF THE GFC AND GSC BESSs

Fig. 19 shows case study 5, in which GFC is recharged until its maximum battery voltage value V_{batmax} is achieved (i.e., occuring at 33.5 s). When $V_{batmax} = 476\ V$, the "Battery voltage control" scheme of the GFC unit increases the frequency of the MG to a value between f_{max} and f_{limit}, driving the GFdC unit to curtail its output power once more. Thus, the GFC unit maintains the recharging procedure with battery voltage below its maximum value, and with a reduced current, characterizing operation within the "Power curtailment" region. Note that the GFC and GSC units are recharged with currents that are proportional to their rated powers, and the two battery banks show very similar dynamics, achieving their maximum values practically at the same time.

It is worth reinforcing that the maximum battery voltage of the GSC unit is controlled autonomously. For instance, Fig. 20 zooms the previous result to show the reduction of input power of the GSC unit when its battery voltage reaches the maximum limit of 476 V. Note that, in 35.46 s, the GSC unit is consuming an active power of $-5062\ W$ when the maximum battery voltage is reached. Thereafter, in 37.88 s, the converter power is reduced to $-3129\ W$ to maintain the

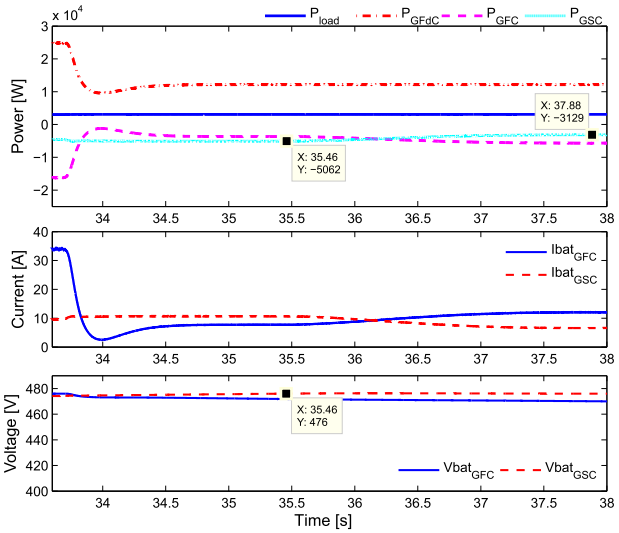

FIGURE 20. Case study 5 - maximum voltage control of GSC battery.

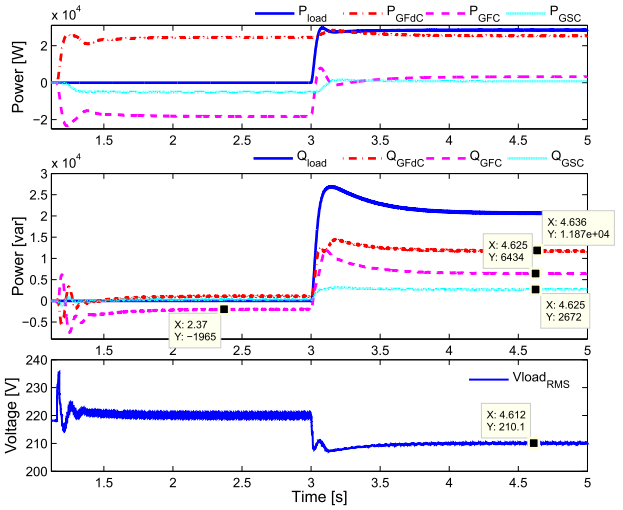

FIGURE 22. Case study 6 - Reactive power sharing simulation with modified droop control.

battery voltage within the acceptable limit and in cohesion with the operation of the GFC and GFdC units.

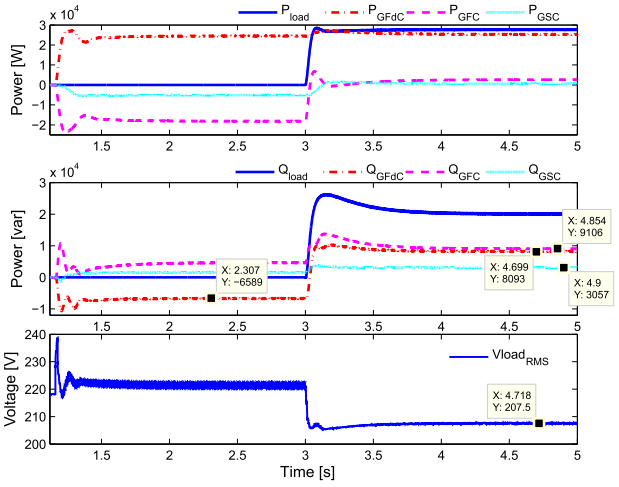

FIGURE 21. Case study 6 - Reactive power sharing simulation with conventional droop control.

E. REACTIVE POWER SHARING BASED ON MODIFIED DROOP CONTROL

This final scenario (i.e., case study 6) shows simulations with an RL load aiming at assessing the reactive power–sharing capability of the current- and voltage-controlled converters. The conventional droop control technique is considered and compared with the modified droop strategy proposed within this article. Thus, Fig. 21 presents the simulation results adopting conventional droop control, while Fig. 22 shows the operation considering the proposed modified version of (1). In both simulated cases, the converters are connected at 1.15 s, without the presence of loads, and at the instant 3 s, the same RL load of the previous case is connected, presenting power factor of 0.8.

For the classic droop method, Fig. 21 demonstrates how that the provision of reactive power by the converters is strongly influenced by the line impedances. Consequently, as expected, the reactive power supplied by the converters are not proportional to their rated powers. It is noticed, for instance, that Q_{GFC} is greater than Q_{GFdC}, while the nominal power of the GFdC unit is greater than that of the GFC. Another inconvenience of the conventional droop is that, during the no load condition, there is a significant amount of unwanted reactive power circulation among converters, with a value of up to 6 *kVAr* for the GFdC unit. In addition, the voltage at the load bus is inherently affected, presenting a value beyond the 5% deviation range defined in Table 2.

On the contrary, by analyzing the operation considering the modified droop control in Fig. 22, it can be verified that the reactive power flowing among converters is reduced in relation to the above-mentioned classic approach, reaching a maximum value of 2 *kVAr* for the GFC unit during the no load condition. When a load step occurs at 3 s, the influence of the line impedances is also reduced, and the reactive power sharing among converters presents reasonable proportionality. Moreover, the voltage in the load bus is adequately regulated, and stays within the desired range.

V. CONCLUSION

This article presented a decentralized control approach for autonomous MGs, in which converters of different operational natures (i.e., behaving as current- or voltage-controlled) coexist and take advantage of the concept of AC bus signaling for proper coordination. Thus, grid-forming, grid-feeding, and grid-supporting converters can endure synergistic operation based on different droop control curves proposed within this article. As a consequence, when dispersed converters are properly managed, power balance among the MG existing entities and automatic prioritization of renewable-based generation from non-dispatchable sources are achieved.

By proposing a charging and discharging control scheme, it was demonstrated that overcurrents and overvoltages can be avoided, to ensure the reliable operation of BESSs, which consequently prolongs their lifespan. In addition, the control strategy supports the converters of such BESSs to be driven either under current- or voltage-controlled modes. The complete design of control loops and droop operating curves of converters were thoroughly demonstrated. Furthermore, novel droop-based equations (i.e., (1) and (3)) were proposed, based on the line resistance voltage drop compensation, to mitigate the influence of mismatching line impedances on reactive power sharing among converters. Several simulations results were presented to certify the effectiveness of the approach and its applicability to the control of an autonomous and inverter-dominated MG.

ACKNOWLEDGMENT

The authors acknowledge the Minas Gerais Research Foundation (FAPEMIG), the Coordenação de Aperfeiçoamento de Pessoal de Nível Superior - Brasil (CAPES) - Finance Code 001, the Sao Paulo Research Foundation (FAPESP) (Grants 2017/24652-8 and 2016/08645-9), and the Research Council of Norway (Grant f261735/H30) for the continuous research support.

REFERENCES

[1] Int. Energy Agency, Paris, France. (2019). *Status of Power System Transformation 2019: Power System Flexibility*. [Online]. Available: https://www.iea.org/reports/status-of-power-system-transformation-2019

[2] E. J. Agnoletto, D. Silva de Castro, R. V. A. Neves, R. Q. Machado, and V. A. Oliveira, "An optimal energy management technique using the ϵ-constraint method for grid-tied and stand-alone battery-based microgrids," *IEEE Access*, vol. 7, pp. 165928–165942, 2019.

[3] Y. Han, H. Li, P. Shen, E. A. A. Coelho, and J. M. Guerrero, "Review of active and reactive power sharing strategies in hierarchical controlled microgrids," *IEEE Trans. Power Electron.*, vol. 32, no. 3, pp. 2427–2451, Mar. 2017.

[4] R. Zamora and A. K. Srivastava, "Controls for microgrids with storage: Review, challenges, and research needs," *Renew. Sustain. Energy Rev.*, vol. 14, no. 7, pp. 2009–2018, Sep. 2010.

[5] J. M. Guerrero, M. Chandorkar, T.-L. Lee, and P. C. Loh, "Advanced control architectures for intelligent microgrids—Part I: Decentralized and hierarchical control," *IEEE Trans. Ind. Electron.*, vol. 60, no. 4, pp. 1254–1262, Apr. 2013.

[6] W. Kang, M. Chen, B. Li, F. Chen, W. Lai, H. Lin, and B. Zhao, "Distributed reactive power control and SOC sharing method for battery energy storage system in microgrids," *IEEE Access*, vol. 7, pp. 60707–60720, 2019.

[7] S. Y. Mousazadeh Mousavi, A. Jalilian, M. Savaghebi, and J. M. Guerrero, "Autonomous control of current- and voltage-controlled DG interface inverters for reactive power sharing and harmonics compensation in islanded microgrids," *IEEE Trans. Power Electron.*, vol. 33, no. 11, pp. 9375–9386, Nov. 2018.

[8] J. Rocabert, A. Luna, F. Blaabjerg, and P. Rodríguez, "Control of power converters in AC microgrids," *IEEE Trans. Power Electron.*, vol. 27, no. 11, pp. 4734–4749, Nov. 2012.

[9] T. Dragičević and Y. Li, "AC and DC microgrid control," in *Control of Power Electronic Converters and Systems*, F. Blaabjerg, Ed. New York, NY, USA: Academic, 2018, pp. 167–200. [Online]. Available: http://www.sciencedirect.com/science/article/pii/B978012816136400018X

[10] H. Han, X. Hou, J. Yang, J. Wu, M. Su, and J. M. Guerrero, "Review of power sharing control strategies for islanding operation of AC microgrids," *IEEE Trans. Smart Grid*, vol. 7, no. 1, pp. 200–215, Jan. 2016.

[11] U. Datta, A. Kalam, and J. Shi, "Battery energy storage system for aggregated inertia-droop control and a novel frequency dependent state-of-charge recovery," *Energies*, vol. 13, no. 8, pp. 1–18, 2020.

[12] J. Kim, J. M. Guerrero, P. Rodriguez, R. Teodorescu, and K. Nam, "Mode adaptive droop control with virtual output impedances for an inverter-based flexible AC microgrid," *IEEE Trans. Power Electron.*, vol. 26, no. 3, pp. 689–701, Mar. 2011.

[13] Q.-C. Zhong and Y. Zeng, "Universal droop control of inverters with different types of output impedance," *IEEE Access*, vol. 4, pp. 702–712, 2016.

[14] A. H. Yazdavar, M. A. Azzouz, and E. F. El-Saadany, "A novel decentralized control scheme for enhanced nonlinear load sharing and power quality in islanded microgrids," *IEEE Trans. Smart Grid*, vol. 10, no. 1, pp. 29–39, Jan. 2019.

[15] A. Micallef, M. Apap, C. Spiteri-Staines, and J. M. Guerrero, "Performance comparison for virtual impedance techniques used in droop controlled islanded microgrids," in *Proc. Int. Symp. Power Electron., Electr. Drives, Autom. Motion (SPEEDAM)*, Jun. 2016, pp. 695–700.

[16] H. Xin, R. Zhao, L. Zhang, Z. Wang, K. P. Wong, and W. Wei, "A decentralized hierarchical control structure and self-optimizing control strategy for F-P type DGs in islanded microgrids," *IEEE Trans. Smart Grid*, vol. 7, no. 1, pp. 3–5, Jan. 2016.

[17] L. Zhang, H. Xin, Z. Wang, and D. Gan, "A decentralized quasi-hierarchical control scheme for droop-controlled AC island microgrids," in *Proc. IEEE Power Energy Soc. Gen. Meeting (PESGM)*, Jul. 2016, pp. 1–5.

[18] Y. Han, M. Yang, P. Yang, L. Xu, X. Fang, K. Zhang, and F. Blaabjerg, "Reduced-order model for dynamic stability analysis of single-phase islanded microgrid with BPF-based droop control scheme," *IEEE Access*, vol. 7, pp. 157859–157872, 2019.

[19] H. R. Baghaee, M. Mirsalim, and G. B. Gharehpetian, "Power calculation using RBF neural networks to improve power sharing of hierarchical control scheme in multi-DER microgrids," *IEEE J. Emerg. Sel. Topics Power Electron.*, vol. 4, no. 4, pp. 1217–1225, Dec. 2016.

[20] L. Zhang, H. Zheng, Q. Hu, B. Su, and L. Lyu, "An adaptive droop control strategy for islanded microgrid based on improved particle swarm optimization," *IEEE Access*, vol. 8, pp. 3579–3593, 2020.

[21] X. Huang, K. Wang, J. Qiu, L. Hang, G. Li, and X. Wang, "Decentralized control of multi-parallel grid-forming DGs in islanded microgrids for enhanced transient performance," *IEEE Access*, vol. 7, pp. 17958–17968, 2019.

[22] N. L. Diaz, J. C. Vasquez, and J. M. Guerrero, "A communication-less distributed control architecture for islanded microgrids with renewable generation and storage," *IEEE Trans. Power Electron.*, vol. 33, no. 3, pp. 1922–1939, Mar. 2018.

[23] D. Wu, F. Tang, T. Dragicevic, J. C. Vasquez, and J. M. Guerrero, "A control architecture to coordinate renewable energy sources and energy storage systems in islanded microgrids," *IEEE Trans. Smart Grid*, vol. 6, no. 3, pp. 1156–1166, May 2015.

[24] D. Wu, F. Tang, T. Dragicevic, J. C. Vasquez, and J. M. Guerrero, "Autonomous active power control for islanded AC microgrids with photovoltaic generation and energy storage system," *IEEE Trans. Energy Convers.*, vol. 29, no. 4, pp. 882–892, Dec. 2014.

[25] D. Wu, F. Tang, T. Dragicevic, J. C. Vasquez, and J. M. Guerrero, "Coordinated primary and secondary control with frequency-bus-signaling for distributed generation and storage in islanded microgrids," in *Proc. 39th Annu. Conf. IEEE Ind. Electron. Soc. (IECON)*, Nov. 2013, pp. 7140–7145.

[26] M. Kamat and S. S. Khule, "Energy balance in AC is-landed micro-grid by frequency bus signaling method," *Int. Res. J. Eng. Technol.*, vol. 4, no. 7, pp. 2764–2776, 2017.

[27] B. Liu, T. Wu, Z. Liu, and J. Liu, "A small-AC-signal injection-based decentralized secondary frequency control for droop-controlled islanded microgrids," *IEEE Trans. Power Electron.*, vol. 35, no. 11, pp. 11634–11651, Nov. 2020.

[28] X. Wu, C. Shen, and R. Iravani, "A distributed, cooperative frequency and voltage control for microgrids," *IEEE Trans. Smart Grid*, vol. 9, no. 4, pp. 2764–2776, Jul. 2018.

[29] J. G. de Matos, F. S. F. e Silva, and L. A. de S. Ribeiro, "Power control in AC isolated microgrids with renewable energy sources and energy storage systems," *IEEE Trans. Ind. Electron.*, vol. 62, no. 6, pp. 3490–3498, Jun. 2015.

[30] M. Sorouri, M. R. Shakarami, and J. Soltani, "Autonomous active power control for an islanded AC microgrid using improved bus signaling method," *Int. J. Electr. Power Energy Syst.*, vol. 113, pp. 549–563, Dec. 2019.

[31] H. J. Moon, Y. J. Kim, J. W. Chang, and S. Moon, "Decentralised active power control strategy for real-time power balance in an isolated microgrid with an energy storage system and diesel generators," *Energies*, vol. 12, no. 3, pp. 1–2, 2019.

[32] L. S. de Araujo, M. G. Villalva, and T. G. Siqueira, "Autonomous microgrid with energy storage system," in *Proc. IEEE 26th Int. Symp. Ind. Electron. (ISIE)*, Jun. 2017, pp. 57–62.
[33] *Voltage Characteristics of Electricity Supplied by Public Distribution System*, Standard EN50160, CENELEC, 2001.
[34] J. M. Guerrero, J. Matas, L. Garcia de Vicuna, M. Castilla, and J. Miret, "Decentralized control for parallel operation of distributed generation inverters using resistive output impedance," *IEEE Trans. Ind. Electron.*, vol. 54, no. 2, pp. 994–1004, Apr. 2007.
[35] H. Liu, Y. Chen, S. Li, and Y. Hou, "Improved droop control of isolated microgrid with virtual impedance," in *Proc. IEEE Power Energy Soc. Gen. Meeting*, 2013, pp. 1–5.
[36] U. N. Patel, D. Gondalia, and H. H. Patel, "Modified droop control scheme for load sharing amongst inverters in a micro grid," *Adv. Energy Res.*, vol. 3, no. 2, pp. 81–95, Jun. 2015.
[37] *Procedimentos de Distribuição de Energia Elétrica no Sistema Elétrico Nacional (PRODIST): Módulo 8–Qualidade da Energia Elétrica*, ANEEL Resolução Normativa 469, 2012.
[38] Z. M. Salameh, M. A. Casacca, and W. A. Lynch, "A mathematical model for lead-acid batteries," *IEEE Trans. Energy Convers.*, vol. 7, no. 1, pp. 93–98, Mar. 1992.
[39] S. Buso and P. Mattavelli, *Digital Control in Power Electronics*. San Rafael, CA, USA: Morgan & Claypool, 2006.
[40] S. Deckmann, F. Marafão, and M. Pádua, "Single and three-phase digital pll structures based on instantaneous power theory," in *Proc. COBEP*, 2003, pp. 225–230.
[41] L. S. de Araujo, D. I. Narvaez, M. G. Villalva, and T. G. de Siqueira, "Multi-converters droop control in single-phase microgrid," in *Proc. IEEE 8th Int. Symp. Power Electron. Distrib. Gener. Syst. (PEDG)*, Apr. 2017, pp. 1–6.

LUCAS SAVOI DE ARAUJO (Graduate Student Member, IEEE) received the bachelor's degree in electrical engineering from the Federal University of Uberlandia, in 2013, and the master's degree in electrical engineering from the University of Campinas, in 2017. He is currently pursuing the Ph.D. degree in electrical engineering with the Federal University of Minas Gerais (UFMG). He has an industry experience as a project engineer. His research interests include power electronics, renewable energy, distributed generation, smart and microgrids, energy storage systems, and electric vehicles.

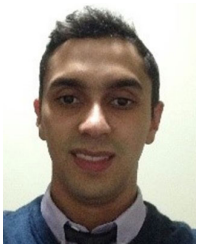

AUGUSTO M. DOS SANTOS ALONSO (Graduate Student Member, IEEE) received the B.S. degree in automation and control engineering from the Federal University of Ouro Preto, Brazil, in 2014, with a sandwich period at The University of New Mexico, USA, from 2012 to 2013, and the M.S. degree in electrical engineering from Sao Paulo State University (UNESP), Brazil, in 2018. He is currently pursuing the double Ph.D. degree at UNESP, as a FAPESP Scholar, and at the Norwegian University of Science and Technology, Norway. His current research interests include the control of grid-tied converters, microgrid control, power quality, and energy policies. In 2019, he was a recipient of the Brazilian Power Electronics Society Award for the best M.S. thesis of the year.

DANILO IGLESIAS BRANDAO (Member, IEEE) received the Ph.D. degree in electrical engineering from the University of Campinas, Brazil, in 2015. He was a Visiting Scholar with the Colorado School of Mines, USA, in 2009 and 2013, and also with the University of Padova, Italy, in 2014, and a Guest Professor with the Norwegian University of Science and Technology, Norway, in 2018 and 2020. He is currently an Assistant Professor with the Federal University of Minas Gerais with the Graduate Program in electrical engineering. His current research interests include the control of grid-tied converters and microgrids.

Dr. Brandao is a member of SOBRAEP.